

EVALUATION OF THE CRITICAL TIMES FOR THE CRACK SUSCEPTIBILITY COEFFICIENT CALCULATION

Taishi Matsushita , Mohammadreza Zamani and Anders E. W. Jarfors
School of Engineering, Jönköping University, 551 11 Jönköping, Sweden

Andrej Kump

NovaCast Systems AB, 372 38 Ronneby, Sweden

Copyright © 2023 The Author(s)
<https://doi.org/10.1007/s40962-023-01083-w>

Abstract

The objective of the present study is to evaluate the hot tearing tendency based on the Clyne and Davies model by evaluating the critical times which can be obtained using a newly developed method. A method to determine the critical times required to calculate the crack susceptibility was presented based on the measurement results with Al–Si alloys, and the method to calculate the crack susceptibility coefficient was presented. In the newly developed method named “Signal intensity method,” signals were generated by tapping the edge of a waveguide which is immersed in molten and solidifying sample and the critical solid

fractions were obtained from the signal intensity change. The conventional thermal analysis was also performed simultaneously and the corresponding critical points were identified. The method shown in the present study will enable the determination of the crack susceptibility coefficient with higher accuracy.

Keywords: crack susceptibility coefficient, hot tear, aluminium alloys, signal intensity

Introduction

The high rejection rate of the specific aluminum alloys due to hot tearing is recognized as a serious problem for several decades, and it is desired to improve manufacturing yield by reducing the rejection rate. As a first step to achieve it, some indexes to describe the vulnerability to hot cracking were suggested in the past. There are some models, which focus on the mechanical properties, to describe the susceptibility of the cracking,¹ and these models can be classified into (1) Stress-based criteria,^{2–6} (2) Strain-based criteria^{2,7–9} and (3) Strain-rate-based criteria.^{10–16} These models may be combined as shown in Ref. [17] It is known that for the alloys which contains enough amount of eutectics, the hot tears are healed through the filling of the cracks with the remained liquid. For example, in the Rappaz–Drezet–Gremaud Model,¹² influence of the healing on the tensile deformation is accounted by considering the mass balance between the solid and liquid phases.

Apart from the mechanical aspects, there are some models which focus on the phase changes during solidification. A widely known index is the Crack Susceptibility Coefficient (CSC) which was suggested by Clyne and Davies.¹⁸ The above-mentioned mechanical property-based models are often compared with the Clyne and Davies model.^{19,20} Clyne and Davies assumed that the system becomes most vulnerable to cracking at the end of the solidification process (between solid fraction 0.9 and 0.99) since the stress can not be released. By taking the ratio of the time to pass this vulnerable range, t_V , and the time which is available for the stress relaxation (between solid fraction 0.40 and 0.9), t_R , the CSC was defined, i.e., $CSC = t_V/t_R$. The criteria of the solid fraction are not strongly supported by theories, but in addition to the relatively simple concept and easiness of the calculation, the experimental results were often reasonably explained with this model; and thus, the model is still used even today.

Since the Clyne–Davies model is relatively simple and based on many assumptions, some modified models have been suggested. Katgerman²¹ considered the influence of

the casting rate and ingot diameter apart from the composition based on the Clyne–Davies model. Easton et al.²² suggested an index to compare the hot tearing tendency between alloys by taking the integral of the solid fraction from coherency temperature to coalescence temperature to overcome the too simple and rough assumptions of the Clyne–Davies model.

As suggested by Katgerman²¹ and modified by Djurdjevic and Huber,²³ at the time when the stress relaxation range start, i.e., solid fraction 0.4 in the Clyne–Davies model, corresponds to the dendrite coherency point (the point at which the dendrite tips impinge on the neighboring dendrite). They have also pointed out that at the time when the vulnerable range start (solid fraction 0.9 in the Clyne–Davies model) corresponds to the “rigidity point.” According to their definition, when the system reached the “rigidity point,” the melt permeability will be significantly decreased due to the lower melt temperature and narrower dendrite channels.

In general, there are two types of methods to determine the dendrite coherency point. A method is thermal analysis,^{24,25} i.e., the coherency point might be determined from the first, second and/or even third derivatives of the cooling curve, or from the temperature difference between the center position and wall side. Another method is the analysis of rheological behavior. In this method, a kind of viscosity measurement by the rotating bob method will be performed,^{23,26} and the dendrite coherency point might be determined from the shear stress (viscosity) change. Also, Djurdjevic and Huber²³ investigated the rigidity point as together with the coherency point through the rheological analysis.

As one can easily imagine, the solid fraction at the coherency and rigidity points depends on the shape of the solid phase, morphology of the dendrite, grain size, etc., and thus the physical property measurement is more desirable than thermal analysis. Since the attenuation of the signal intensity is proportional to the degree of the network of the solid phase and solid/liquid fraction, in the present study, the relative intensity change of the wave generated

by the piezoelectric element was observed during the solidification process to determine the critical times. The obtained critical times were used to calculate the Crack Susceptibility Coefficient in a similar way with the Clyne–Davies model. The two-thermocouple method, which was commonly introduced by researchers,^{23,24,26,27} was employed to investigate the relationship with the signal intensity change.

Experimental

Materials

A “pure” aluminum (99.9 mass%Al), two hypoeutectic Al–Si alloys, an Al–Si alloy close to the eutectic, a hypereutectic Al–Si alloy, and two commercial aluminum alloys were supplied for the experiments. Four Al–Si alloys were prepared by adding silicon (99.9 mass%Si) into pure aluminum using an induction furnace. The composition of the alloys was analyzed by a spectrometer. The composition of alloys is summarized in Table 1.

Apparatus

A schematic illustration of the apparatus to measure the signal intensity change during the solidification is shown in Figure 1. The apparatus consists of a crucible made of croning sand, the waveguides to send and receive the signals, a piezoelectric element to tap the edge of the waveguide and send the signals, and data loggers. The waveguides are made of low carbon steel, and the length and diameter of the waveguides are 130 mm and 4 mm, respectively. The distance between the waveguides was set as 15 mm. A thermocouple is located at the center of the crucible, and another thermocouple is located at the wall side at the same height. For the measurement of cooling curves and calculation of its derivatives, a commercially available metallurgical process control system named ATAS MetStar (NovaCast Systems AB), which consists of two thermocouples and a data logging system, was employed.

Table 1. Composition of the Alloys (Mass%)

| Sample | Si | Fe | Mn | Mg | Zn | Ti | V | Al |
|--------------------|------|------|------|------|------|------|------|---------|
| Al–1.2Si | 1.2 | 0.03 | | | | | | Balance |
| Al–7.2Si | 7.2 | 0.06 | | | | | | Balance |
| Al–12.1Si | 12.1 | 0.07 | | | | | | Balance |
| Al–19.1Si | 19.1 | 0.07 | | | | | | Balance |
| Commercial alloy 1 | 10.1 | 0.20 | 0.02 | | | | | Balance |
| Commercial alloy 2 | 0.81 | 0.34 | 0.55 | 0.27 | 0.05 | 0.13 | 0.01 | Balance |

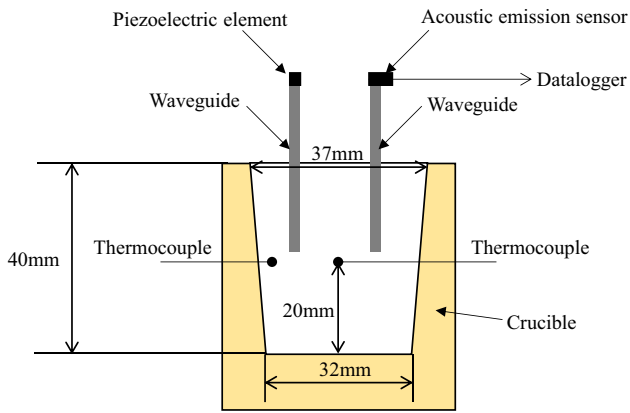


Figure 1. A schematic illustration of the experimental setup.

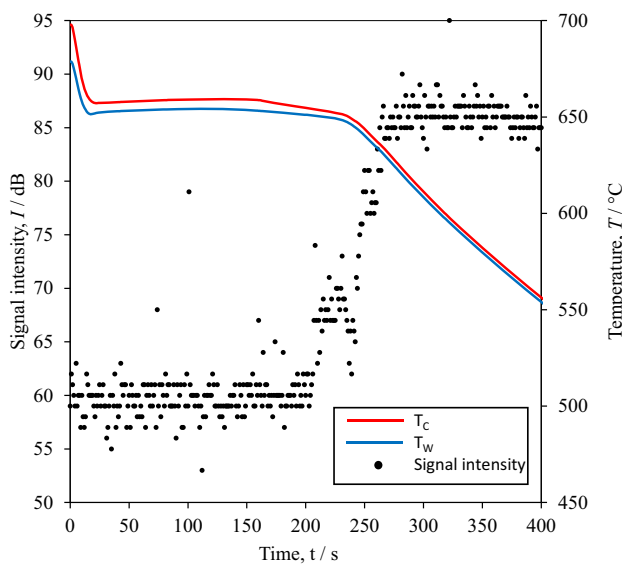


Figure 2. Signal intensity, temperatures at the center and wall side for "Pure" Al.

Procedure

The edge of the waveguide was tapped with 5 Hz using the piezoelectric element. After the tapping was started, six kilograms Al-Si alloy was melted at 750 °C in a resistance furnace and the molten alloy which is required to fill the above-mentioned crucible was taken from there using a ladle and poured into the crucible. The signal intensity of the tapping was continuously measured using an acoustic emission sensor and logged. Simultaneously, the temperature at the center and the side positions were measured using two thermocouples.

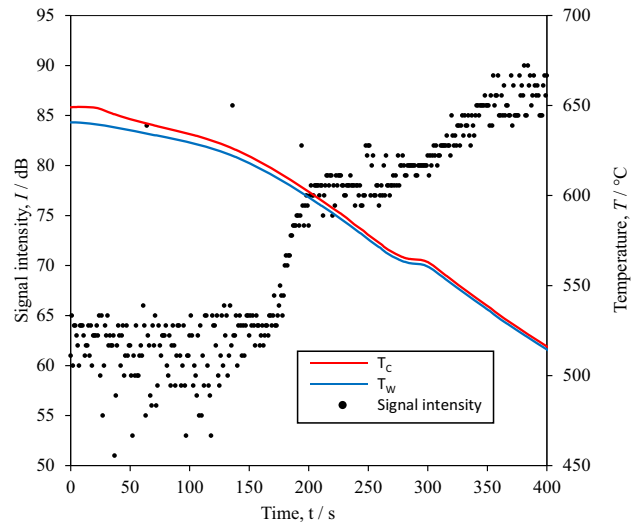


Figure 3. Signal intensity, temperatures at the center and wall side for Al-1.2Si (Solidus temperature: 591 °C, Liquidus temperature: 653 °C).

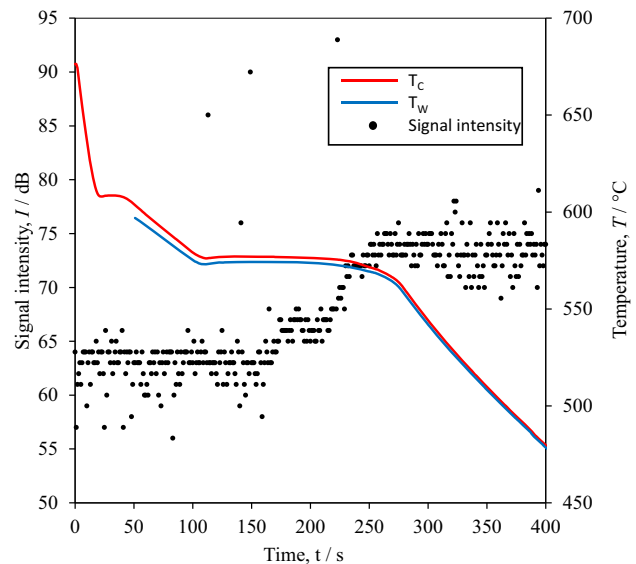


Figure 4. Signal intensity, temperatures at the center and wall side for Al-7.2Si (Solidus temperature: 575 °C, Liquidus temperature: 615 °C).

Results and Discussion

Signal Intensity

The signal intensity and the temperatures at center (T_C) and wall side (T_W) change against time for Pure Al, 1.2%Si, 7.2%Si, 12.1%Si and 19.1%Si alloys are shown in Figures 2, 3, 4, 5 and 6. The time at which the melt is poured into the crucible is taken as zero.

As can be seen from Figures 2, 3, 4 and 5, for the hypoeutectic alloys, the signal intensity was increased stepwise during the solidification as shown in Figure 7. In the beginning, the signal intensity was constant (I_B) up to

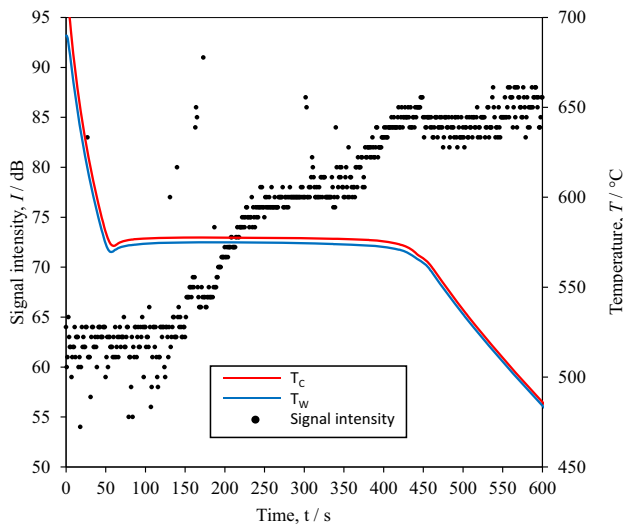


Figure 5. Signal intensity, temperatures at the center and wall side for Al–12.1Si (Solidus temperature: 575 °C, Liquidus temperature: 580 °C).

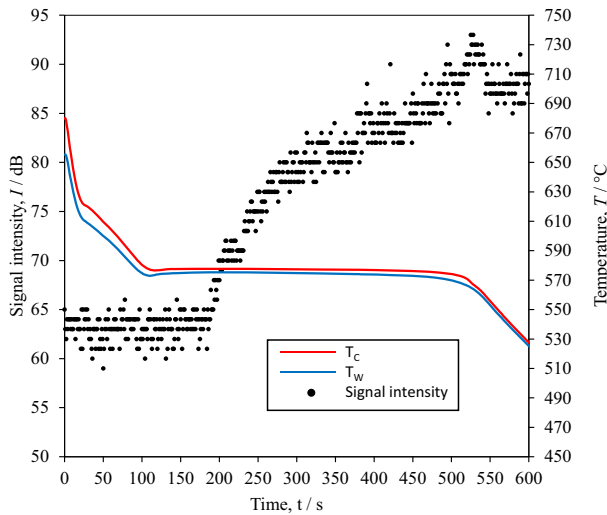


Figure 6. Signal intensity, temperatures at the center and wall side for Al–19.1Si (Solidus temperature: 575 °C, Liquidus temperature: 676 °C).

t_1 . In the initial stage up to t_1 , the cast metal is fully molten state or the fraction of solid is low; and thus, it shows relatively low and constant intensity.

At t_1 , the network of the dendrite between two waveguides is established, and the signal start to transfer through the dendrite (solid phase). The intensity increases between t_1 and t_2 , with increasing of the degree of the network of the solid phase due to the increasing of solid fraction. In this period, the rearrangement of the growing solid dendrites is possible and it corresponds to the time for the “mass feeding” of the Clyne–Davies model. After this stage, a plateau appears between t_2 and t_3 . In this stage, the hard impingement stops the growth of the impinging crystal, and this will fill the space through new nucleation and growth

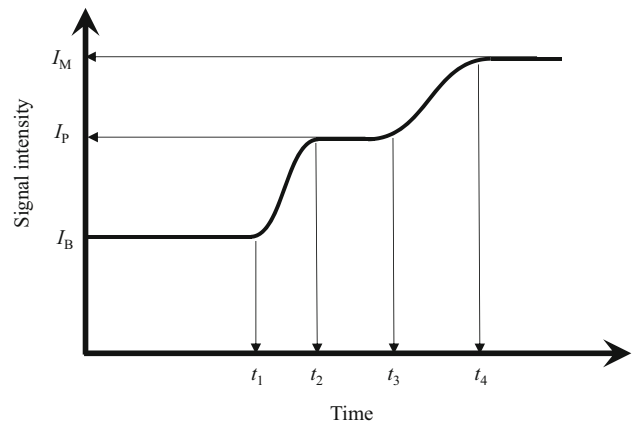


Figure 7. Schematic of the signal intensity change during the solidification of hypoeutectic alloys.

until all crystals have impinged at t_3 , and thus the degree of dendrite network, in other words, the signal intensity will become constant between t_2 and t_3 . During this period, the liquid movement between the dendrite is still possible and it allows the stress relaxation, i.e., it corresponds to the time for the “liquid feeding” of the Clyne–Davies model.

After t_3 , the coarsening becomes dominant, which allows better transduction of signals until the system is fully solidified at t_4 . In this stage, it can be considered as the liquid phase as interdendritic film.

On the other hand, in the case of hypereutectic alloy (19.1%Si), such stepwise increasing of the signal intensity, i.e., the plateau between t_2 and t_3 was not observed (Figure 6). In the case of hypereutectic alloy, after the primary phase is formed as particles, the degree of solid phase network will be increased, i.e., the signal intensity will be increased with increasing of the fraction of the eutectic phase.

Crack Susceptibility Coefficient

As mentioned above, the time between t_1 and t_3 corresponds to the time available for stress relief process, and the time between t_3 and t_4 corresponds to the vulnerable time period of the Clyne–Davies model. Therefore, the Crack Susceptibility Coefficient (CSC) can be calculated by the following equation based on the finding by Djurdjevic and Huber.²³

$$\text{CSC} = \frac{t_4 - t_3}{t_3 - t_1} \quad \text{Eqn. 1}$$

In the Clyne–Davies model, to find out the period which is available for the stress relaxation and the period for the vulnerable range, the critical solid fraction must be set based on some assumptions. However, in the present method, one can find the period which is available for

Table 2. Characteristic Times and CSC Values

| Sample | t_1 (s) | t_3 (s) | t_4 (s) | CSC (Present study) | CSC (Clyne–Davies model (Thermo- Calc)) |
|---------------|--------------|--------------|--------------|---------------------------|---|
| Al | 194 | 243 | 266 | 0.47 | 0.26 |
| Al– 1.2Si | 174 | 279 | 359 | 0.76 | 0.43 |
| Al– 7.2Si | 157 | 222 | 254 | 0.49 | 0.27 |
| Al– 12.1Si | 136 | 344 | 423 | 0.38 | 0.26 |

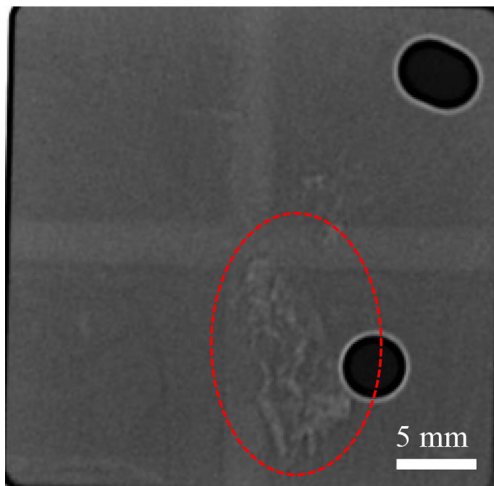


Figure 8. An X-ray image of Al–1.2%Si.

stress relaxation ($t_3 - t_1$) and the period for the vulnerable range ($t_4 - t_3$) from the signal intensity change without knowing the solid fraction. This is an advantage of the present method since the degree of the physical connectivity (dendrite network) depends on not only the solid fraction but also the shape of the solid phase, morphology of the dendrite and grain size.

The characteristic times were read off from Figures 2, 3, 4 and 5 by referring to the change in the upper and lower signal intensities of the band of intensity. I values are summarized in Table 2 together with the calculated CSC. These values have certain reading errors since these values were read off from the graphs, and thus the errors are discussed in Section 4.3

For the comparison, the CSC values by Clyne–Davies model were calculated using Thermo–Calc software (Thermo–Calc 2021a, TCAL7 database), and the values are shown in Table 2. Note that the difference in the absolute CSC values between the present study and the Clyne–Davies model (Thermo–Calc) is not crucial since the parameters used in the calculation are not the same

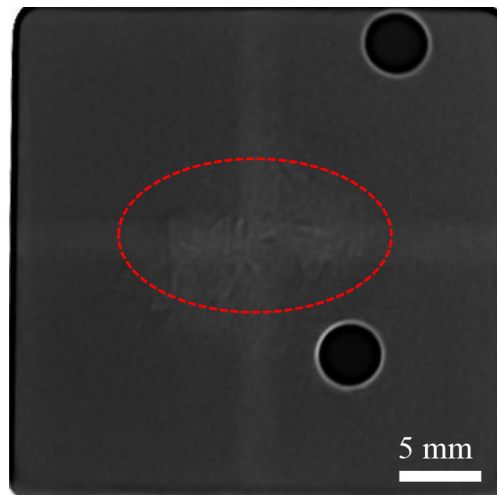


Figure 9. An X-ray image of Al–7.2%Si.

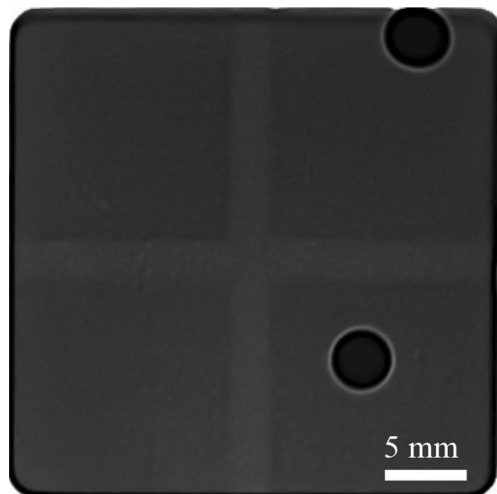


Figure 10. An X-ray image of Al–12.1%Si.

although the basic idea is the same. For the prediction of cracking behavior of different alloys, the relative difference of the CSC values in the same evaluation method should be considered. As can be seen from the CSC values, the trend of the change in CSC value against Si amount is the same in both the results of the present study and Thermo–Calc calculation, i.e., the CSC value increases with increasing of Si up to 1.2 mass% Si and decreases with further increasing of Si.

As can be seen from the calculated CSC values (Table 2), in the case of Al–Si binary system, it is expected that Al–1.2Si (and Al–7.2Si) has a higher risk of hot tearing compared with the other samples. To confirm if the sample has been cracked or not, X-ray images of the samples were taken after the experiments. The X-ray photos were taken from the bottom side of the cast samples. As examples, the X-ray images of Al–1.2Si, Al–7.2%Si and Al–12.1%Si samples are shown in Figures 8, 9 and 10, respectively.

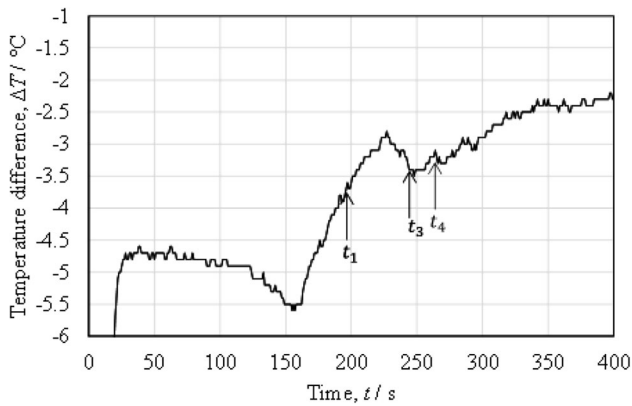


Figure 11. Temperature difference between the center and wall side for "Pure" Al.

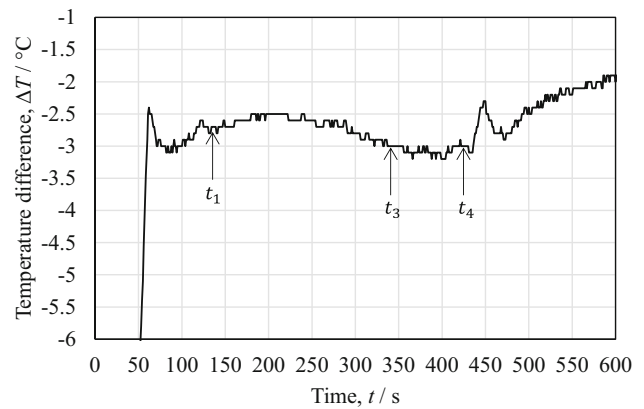


Figure 14. Temperature difference between the center and wall side for Al-12.1Si.

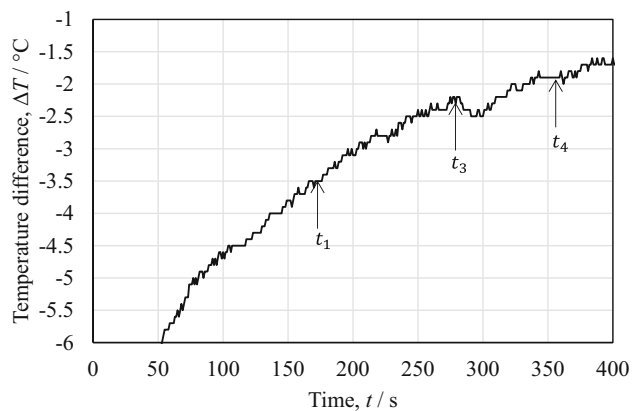


Figure 12. Temperature difference between the center and wall side for Al-1.2Si.

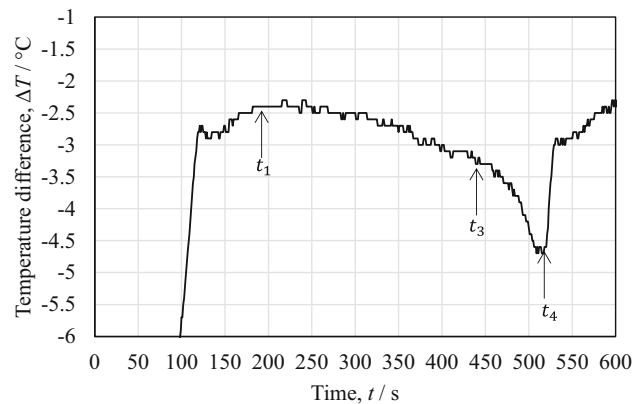


Figure 15. Temperature difference between the center and wall side for Al-19.1Si.

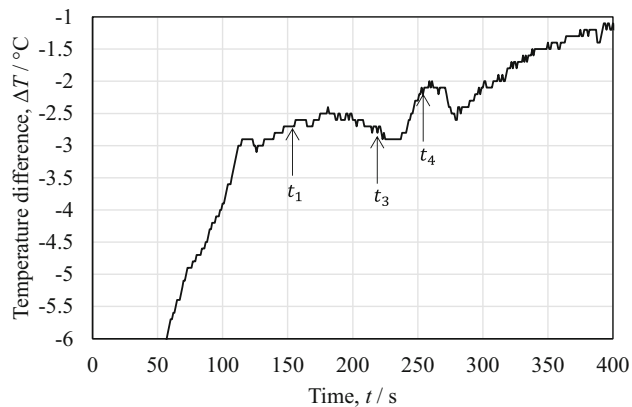


Figure 13. Temperature difference between the center and wall side for Al-7.2Si.

As can be seen in Figures 8 and 9, for the samples which have relatively higher CSC values, the pores and cracks were observed near the center. On the other hand, in the case of Al-12.1%Si sample, such cracks have not been observed (Figure 10).

Temperature Difference, Thermal Analysis and Characteristic Times

To investigate the relationship between the signal intensity change and the thermal behavior, the temperature difference between the center and wall side was plotted against time (Figures 11, 12, 13, 14 and 15). As one can see from Figures 11, 12, 13, 14 and 15, there are no significant correlation between signal intensity change vs. maximum difference between TC-wall and TC-center.

To find out the corresponding characteristic times in the cooling curve, the first and second derivatives of the curves were calculated, and the thermal changes on first and second derivative on thermocouple at center location were found. This event gives us in most cases a close match to the definition of the t_1 point and t_3 point in the signal intensity method. As shown in Figures 16, 17, 18, 19 and 20, the algorithm to determine t_1 point and t_3 point was applied only from cooling curve (central position thermocouple) and its derivatives. The t_1 point is determined when first derivative changes from positive to negative after the

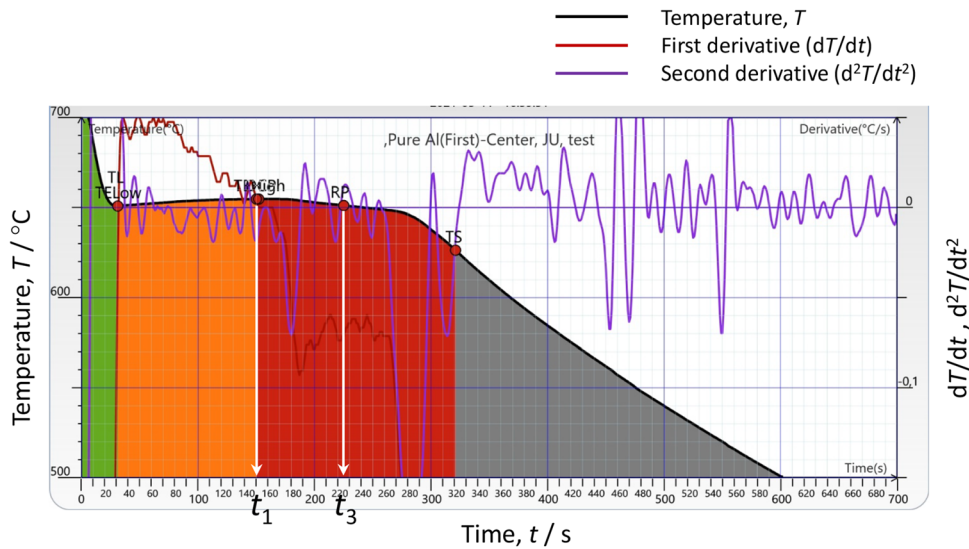


Figure 16. Cooling curve and its derivatives for "pure" Al.

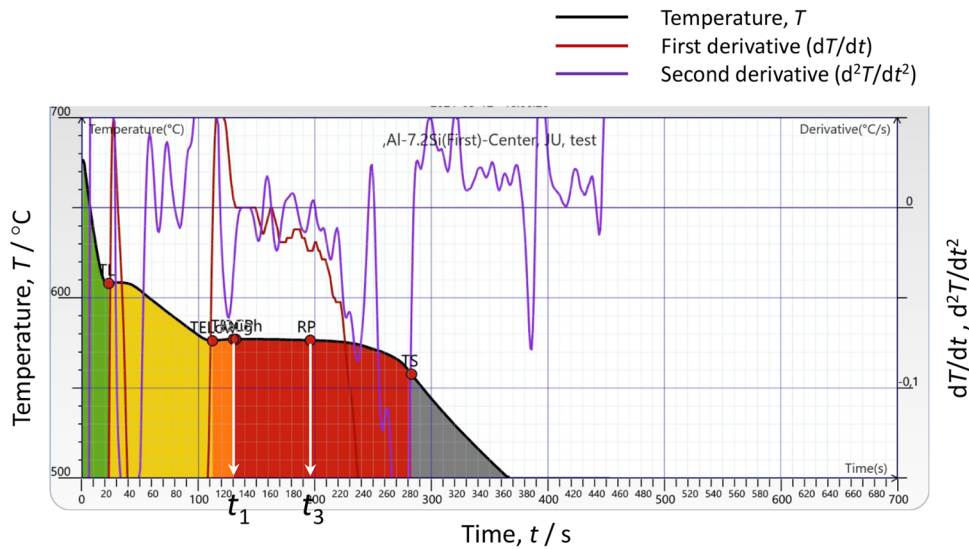


Figure 17. Cooling curve and its derivatives for Al-7.2 Si.

liquidus temperature (TL). While t_3 point is determined in the last gap formed between cooling rate and acceleration before the descent to solidus (Figure 18).

The characteristic times (t_1 and t_3) and corresponding temperatures which were read from first and second derivative are summarized in Table 3.

As can be seen in Tables 2 and 3, for the time t_3 , the time obtained from the signal intensity method reasonably agrees with the time obtained by the thermal analysis. On the other hand, matching of the t_1 between the signal intensity method and TA is moderate. The largest mismatch of t_1 is visible for the commercial alloy 1 case. As one can see in Tables 2 and 3, in the case of Al-Si binary alloys, the t_1 by TA is always shorter than that of the signal intensity method.

Application to the Commercial Alloys

The above-mentioned signal intensity method to determine the characteristic times (t_1 , t_3 and t_4) and CSC has been applied for two commercial aluminum alloys (Commercial alloy 1 and Commercial alloy 2). The intensity change during the solidification process of these two alloys is shown in Figures 20 and 21.

The characteristic times which were read from the signal intensity change and calculated CSC values are summarized in Table 4.

As can be seen in Table 4, Commercial alloy 2 shows a higher CSC value, i.e., it has a higher risk of the cracking, and it agrees with the observation in the real process.

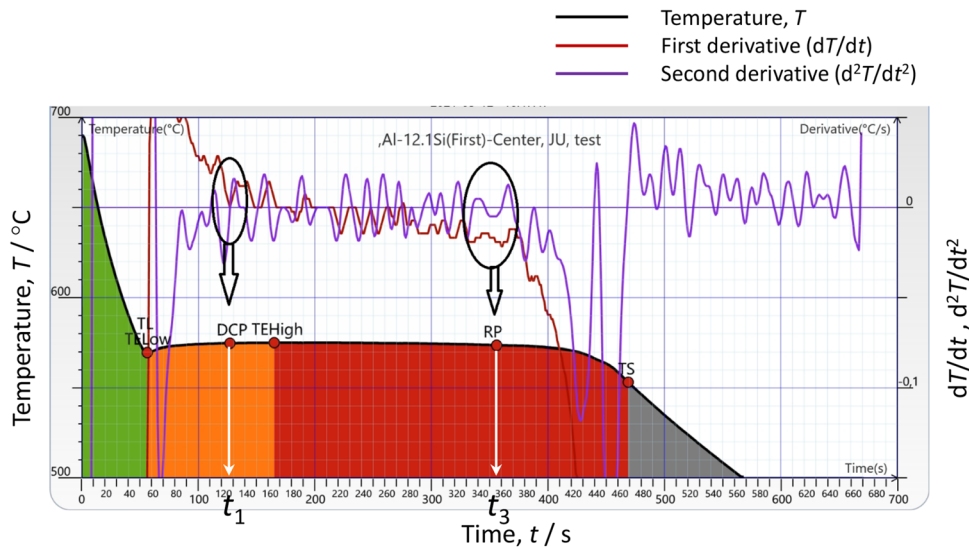


Figure 18. Cooling curve and its derivatives for Al-12.1Si.

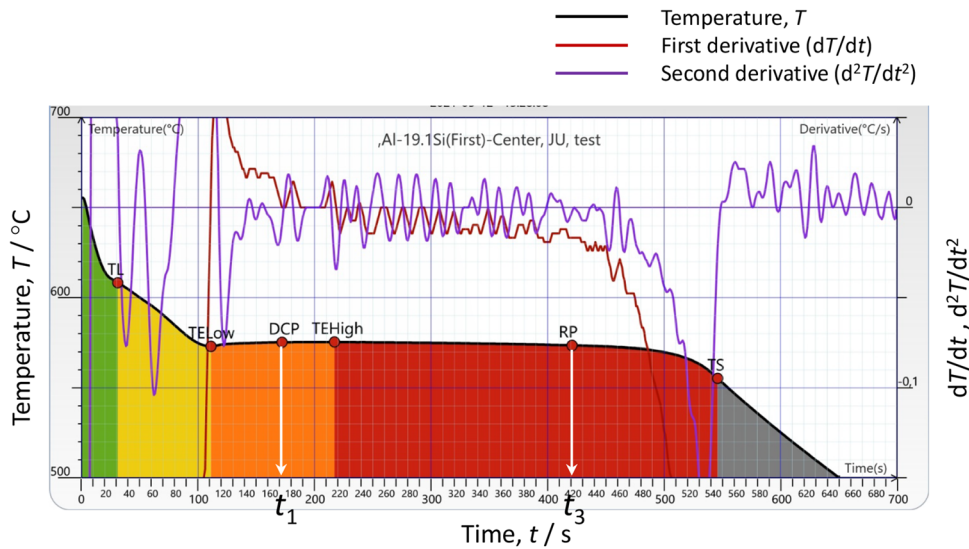


Figure 19. Cooling curve and its derivatives for Al-19.1Si.

The reproducibility of the measurement was confirmed for the Commercial alloy 1. In the repeated experiment, the characteristic times t_1 , t_3 and t_4 became 147 s, 322 s and 432 s, respectively, and the CSC value is 0.63.

The absolute value of these characteristic times will be influenced by the cooling rate (small difference in the cooling rate or difference in the sample size), the distance between the waveguides, etc., but the CSC value, i.e., the ratio of $t_4 - t_3$ and $t_3 - t_1$ will not be influenced since these values are proportionally changed. Comparing the CSC value for the first measurement for Commercial alloy 1, the standard deviation of the CSC value becomes 0.08.

Regarding the influence of the reading error of the characteristic times on the CSC value, for example, if it is assumed that the reading error is ± 5 sec., the error in the

CSC value will become 0.03–0.1 in the case of present experiments. For the on-site measurement in the real process, a shorter measurement time is desired but to decrease the influence of the reading error of the characteristic times on the CSC value, it is desired to use a larger amount of sample so that the duration of the $t_4 - t_3$ and $t_3 - t_1$ becomes longer. The measurement accuracy can also be increased by logging the data with higher frequency.

Conclusions

In the present study, a novel method named “Signal intensity method” to determine the crack susceptibility coefficient (CSC) was proposed, i.e., a periodical signal was generated by tapping the edge of the waveguide, and the intensity change was detected on another waveguide.

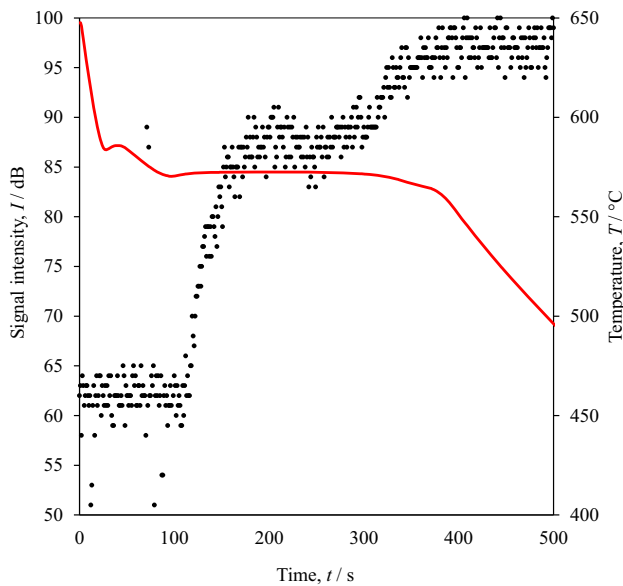


Figure 20. Signal intensity for Commercial alloy 1.

Table 3. Characteristic Times and Temperatures

| | t_1 (s) | Temperature at t_1 (°C) | t_3 (s) | Temperature at t_3 (°C) |
|-----------|--------------|------------------------------|--------------|------------------------------|
| Al | 152 | 655 | 225 | 651 |
| Al–7.2Si | 132 | 577 | 196 | 576 |
| Al–12.1Si | 127 | 575 | 356 | 574 |
| Al–19.1Si | 172 | 572 | 421 | 574 |

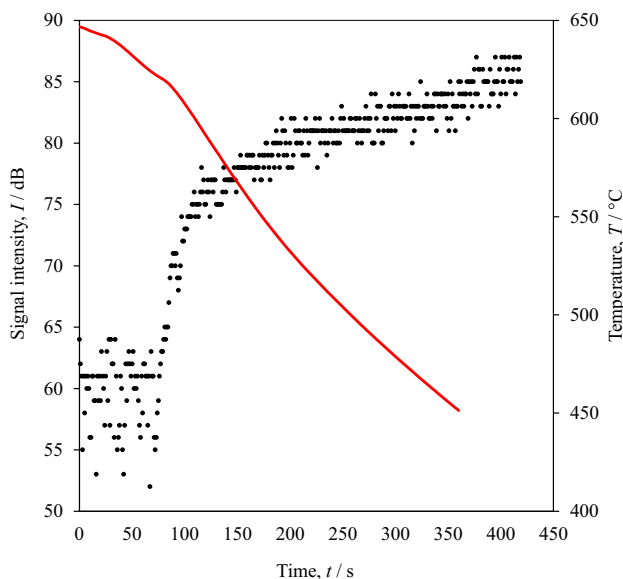


Figure 21. Signal intensity for Commercial alloy 2.

Table 4. Characteristic Times and CSC Values for the Commercial Alloys

| Sample | t_1 (s) | t_3 (s) | t_4 (s) | CSC (Present study) | CSC (Clyne– Davies model (Thermo-Calc)) |
|--------------------|--------------|--------------|--------------|---------------------------|---|
| Commercial alloy 1 | 100 | 287 | 383 | 0.51 | 0.27 |
| Commercial alloy 2 | 76 | 174 | 380 | 2.10 | 0.90 |

The intensity change was measured during the solidification of aluminum alloys, and it was found that the signal intensity increases stepwise in the solidification process. The characteristic times were obtained from the signal intensity changes.

Based on the measured characteristic times, the CSC was calculated, and the results were compared with that of the Clyne–Davies model. The results show a reasonable agreement, and the results were verified by the X-ray observation.

The correspondence of the characteristic times in the conventional method, i.e., the thermal analysis method was also investigated, and it shows reasonable agreement with the time obtained by the present signal intensity method.

Acknowledgments

The authors acknowledge Thermo-Calc Software AB for providing the database for thermodynamic calculations. The authors thank Lundbergs Pressgjuteri for the X-ray photo images and Gränges Sweden AB for providing the materials.

Funding

Open access funding provided by Jönköping University. The Knowledge Foundation supported this work via the project OMQAL with grant number 20180192.

Conflict of interest The authors declare no conflict of interest.

Open Access This article is licensed under a Creative Commons Attribution 4.0 International License, which permits use, sharing, adaptation, distribution and reproduction in any medium or format, as long as you give appropriate credit to the original author(s) and the source, provide a link to the Creative Commons licence, and indicate if changes were made. The images or other third party material in this article are included in the article's Creative Commons licence, unless indicated otherwise in a credit line to the material. If material is not included in the article's Creative Commons licence and your intended use is not permitted by statutory regulation or exceeds the permitted use, you will need to obtain permission directly from the copyright holder. To view a copy of this licence, visit <http://creativecommons.org/licenses/by/4.0/>.

REFERENCES

1. S. Li, D. Apelian, *Inter. Metalcast.* **5**, 23–40 (2011). <https://doi.org/10.1007/BF03355505>.
2. I. I. Novikov, *Goryachelomkost Tsvetnykh Metallov i Splavov (Hot Shortness of Non-Ferrous Metals and Alloys)*, p. 299 (1966).
3. C.H. Dickhaus, L. Ohm, S. Engler, *AFS Trans.* **101**, 677 (1994)
4. D.J. Lahaie, M. Bouchard, *Metall. Mater. Trans. B* **32**, 697 (2001)
5. J. Langlais, J.E. Gruzleski, *Mater. Sci. Forum* **331–337**, 167–172 (2000)
6. J.A. Williams, A.R.E. Singer, *J. Inst. Met.* **96**, 5–12 (1968)
7. Suyitno, W. H. Kool, L. Katgerman, *Light Metals*, pp. 753–758 (2003).
8. L. Zhao, Baoyin, N. Wang, V. Sahajwalla, R.D. Pehlke, *Int. J. Cast Metals Res.* **13**, 167–174 (2000)
9. B. Magnin, L. Maenner, L. Katgerman, S. Engler, *Mater. Sci. Forum* **217–222**, 1209–1214 (1996)
10. D.G. Eskin, Suyitno, L. Katgerman, *Progress Mater. Sci.* **49**, 629–711 (2004)
11. N.N. Prokhorov, *Russ. Cast. Prod.* **2**, 172–175 (1962)
12. M. Rappaz, J.-M. Drezet, M. Gremaud, *Metall. Mater. Trans. A* **30A**, 449–455 (1999)
13. Suyitno, W.H. Kool, L. Katgerman, *Metall. Mater. Trans. A* **36**, 1537–1546 (2005)
14. M. Braccini, C. L. Martin, M. Suéry, Y. Bréchet, *Welding and Advanced Solidification Processes IX*, pp.18–24 (2000).
15. M. M’Hamdi, A. Mo, H.G. Fjær, *Metall. Mater. Trans. A* **37A**, 3069–3083 (2006)
16. A. Stangeland, A. Mo, Ø. Dielsen, D. Eskin, M. M’Hamdi, *Metall. Mater. Trans. A* **35A**, 2903–2915 (2004)
17. S. Li, K. Sadayappan, D. Apelian, *Int. J. Cast Met. Res.* **24**, 88–95 (2011)
18. T.W. Clyne, G.J. Davies, *Br. Foundrym.* **74**, 65–73 (1981)
19. B. Yu, R. Dou, Y. Wang, X. Liu, Z. Wen, J. Wang, *Int. Metalcast.* (2022). <https://doi.org/10.1007/s40962-022-00848-z>
20. M.R. Nasresfahani, B. Niroumand, *Int. Metalcast.* **14**, 538–546 (2020)
21. L. Katgerman, *J. Met.* **34**(2), 46–49 (1982)
22. M.A. Easton, M.A. Gibson, S. Zhu et al., An a priori hot-tearing indicator applied to die-cast magnesium-rare earth alloys. *Metall. Mater. Trans. A* **45**, 3586–3595 (2014)
23. M.B. Djurdjevic, G. Huber, *J. Alloys Compd.* **590**, 500–506 (2014)
24. M.B. Djurdjevic, J.H. Sokolowski, Z. Odanovic, *J. Therm. Anal. Calorim.* **109**, 875–882 (2012)
25. I.V. Gómez, E.V. Viteri, J. Montero, M. Djurdjevic, G. Huber, *Appl. Sci.* **8**, 1236 (2018)
26. N.L.M. Veldman, A.K. Dahle, D.H. StJohn, L. Arnberg, *Metal. Mater. Trans. A* **34A**, 147–155 (2001)
27. S.G. Shabestari, M.H. Ghoncheh, *Metal. Mater. Trans. B* **46B**, 2438–2448 (2015)

Publisher’s Note Springer Nature remains neutral with regard to jurisdictional claims in published maps and institutional affiliations.